**Atmospheric
Chemistry
and Physics**

Size and time-resolved growth rate measurements of 1 to 5 nm freshly formed atmospheric nuclei

C. Kuang[1], **M. Chen**[2], **J. Zhao**[3], **J. Smith**[3], **P. H. McMurry**[2], and **J. Wang**[1]

[1]Atmospheric Sciences Division, Brookhaven National Laboratory, Building 815E, Upton, NY, 11973, USA
[2]Department of Mechanical Engineering, University of Minnesota, 1100 Mechanical Engineering, 111 Church Street SE, Minneapolis, MN 55455, USA
[3]Atmospheric Chemistry Division, National Center for Atmospheric Research, P.O. Box 3000, Boulder, CO 80307, USA

Correspondence to: J. Wang (jian@bnl.gov)

Abstract. This study presents measurements of size and time-resolved particle diameter growth rates for freshly nucleated particles down to 1 nm geometric diameter. Novel data analysis methods were developed, de-coupling for the first time the size and time-dependence of particle growth rates by fitting the aerosol general dynamic equation to size distributions obtained at an instant in time. Size distributions of freshly nucleated total aerosol (neutral and charged) were measured during two intensive measurement campaigns in different environments (Atlanta, GA and Boulder, CO) using a recently developed electrical mobility spectrometer with a diethylene glycol-based ultrafine condensation particle counter as the particle detector. One new particle formation (NPF) event from each campaign was analyzed in detail. At a given instant in time during the NPF event, size-resolved growth rates were obtained directly from measured size distributions and were found to increase approximately linearly with particle size from ∼1 to 3 nm geometric diameter, increasing from 5.5 ± 0.8 to 7.6 ± 0.6 nm h^{-1} in Atlanta (13:00) and from 5.6 ± 2 to 27 ± 5 nm h^{-1} in Boulder (13:00). The resulting growth rate enhancement Γ, defined as the ratio of the observed growth rate to the growth rate due to the condensation of sulfuric acid only, was found to increase approximately linearly with size from ∼1 to 3 nm geometric diameter. For the presented NPF events, values for Γ had lower limits that approached ∼1 at 1.2 nm geometric diameter in Atlanta and ∼3 at 0.8 nm geometric diameter in Boulder, and had upper limits that reached 8.3 at 4.1 nm geometric diameter in Atlanta and 25 at 2.7 nm geometric diameter in Boulder. Nucleated particle survival probability calculations comparing the effects of constant and size-dependent growth indicate that neglecting the strong dependence of growth rate on size from 1 to 3 nm observed in this study could lead to a significant overestimation of CCN survival probability.

1 Introduction

Atmospheric aerosols influence climate and climate change on local to global scales by affecting the atmospheric radiation balance directly through scattering and absorbing incoming solar radiation and indirectly as cloud condensation nuclei (CCN) (Charlson et al., 1992). Atmospheric measurement and modeling studies have shown that new particle formation (NPF), through photochemical reactions of gas-phase precursors, greatly increases the number concentration of atmospheric aerosols, and is often followed by rapid growth of the nucleated aerosol to a CCN-active size, significantly increasing the CCN population (Lihavainen et al., 2003; Kerminen et al., 2005; Spracklen et al., 2008; Kuang et al., 2009). This rapid growth, often many times that of the growth assuming the condensation of sulfuric acid alone (Weber et al., 1997), is neither well understood nor represented in regional and chemical transport models (Pierce and Adams, 2007; Wang and Penner, 2009; Spracklen et al., 2010). This lack of understanding limits the ability to realistically assess the impact of NPF on the global surface CCN population and its contribution to the aerosol indirect effect.

Growth rates based solely on the condensation of sulfuric acid vapor significantly underestimate the observed growth

rate (Sihto et al., 2006; Riipinen et al., 2007; Iida et al., 2008; Kuang et al., 2010; Nieminen et al., 2010) largely because organic compounds are responsible for up to 95 % of the growth (Mäkelä et al., 2001; O'Dowd et al., 2002; Smith et al., 2008, 2010). This enhancement in growth can be characterized by a quantity, Γ, defined as the measured diameter growth rate divided by the diameter growth rate due to the condensation of sulfuric acid, quantifying the contribution of other species to the observed growth. Compiled values of Γ for nanoparticle growth rates measured in diverse environments indicate an average of value of 5 to 10 with values as high as 20 to 50, clearly showing that, on a global level, growth rates of freshly nucleated particles are due to the uptake of species other than sulfuric acid (Kuang et al., 2010).

Particle growth rates reflect the sum of all gas-to-particle conversion processes that contribute to growth, and therefore include important information on chemical processes that affect growth. Chemical models are needed to explain observed growth rates and developing such models will require measurements of gas-phase species that contribute to growth, measurements of particle composition, as well as an understanding of the dependence of observed growth rates on concentrations of the gas-phase precursors. For example, previous research has shown that sulfuric acid condenses on particles at the diffusion limit with an accommodation coefficient close to 1.0 (Jefferson et al., 1997), indicating that the contribution of sulfuric acid to the growth of large particles (>20 nm) can be modeled. Smith and co-workers have shown that alkyl ammonium carboxylate salts, formed by reactions between amines and carboxylic acids, account for 20 to 50 % of observed growth in the atmosphere (Smith et al., 2010), but the mechanism for this process is not yet understood in part because the gas-phase precursors have not been measured. Establishing such chemical models requires accurate information on growth rates. This paper describes methods that can be used to de-couple the dependencies of growth rates on size and time for the smallest (~1 to 5 nm geometric diameter) nucleated particles.

This de-coupling is particularly crucial as it allows for the clear interpretation of observed size-dependent growth as a consequence of the particular particle growth mechanism at work rather than the consequence of time-dependent vapor condensation on the growing aerosol. Early aerosol growth studies developed and applied techniques to obtain, from measured size distributions, size-dependent growth rates of 30 to 600 nm particles growing through gas to particle conversion (Friedlander, 1977; Heisler and Friedlander, 1977; McMurry and Wilson, 1982; McMurry and Grosjean, 1985). As aerosol sizing and counting instrumentation have improved since then (McMurry, 2000), particle growth rates have been obtained for even smaller sizes, down to 3 nm – the conventional size detection limit for measuring the total aerosol (Stolzenburg and McMurry, 1991).

Recently, the development of a scanning mobility particle spectrometer (SMPS) using a diethylene glycol-based ultra-fine condensation particle counter (DEG UCPC) has enabled the first mobility-classified measurements of the complete number size distribution for the total aerosol during an atmospheric nucleation event, bridging the size range from vapor molecules and molecular clusters (<1 nm geometric diameter) to nanoparticles and sub-micrometer particles (Jiang et al., 2011b). While earlier studies have presented sub 3 nm size distributions acquired during nucleation events using activation-sizing techniques (Sipilä et al., 2009; Lehtipalo et al., 2011), mobility-classified size distributions of freshly nucleated aerosol were measured in this study using a DEG UCPC to extend SMPS measurements down to ~1 nm (Jiang et al., 2011a). Such measurements enable the direct determination of not only the rates at which these nuclei are formed, but also the rates at which neutral nuclei as small as 1 nm geometric diameter grow as functions of time and size.

Using size distribution measurements of the total aerosol (neutral and charged) down to ~1 nm geometric diameter, novel data analysis methods were developed in this study to de-couple, for the first time, the size and time-dependence of particle growth rates for freshly nucleated aerosol. While earlier studies have presented evidence for size-dependent growth rates of nucleation mode particles, those results were obtained from size distributions of the ambient ion population and were averaged over particle size and growth time (Hirsikko et al., 2005; Manninen et al., 2009; Yli-Juuti et al., 2011). Methods for obtaining size and time-resolved growth rates are presented, along with insights into the processes of nucleation and growth provided by these measurements.

2 Experimental

2.1 Measurements

Analyzed nucleation events were acquired during two intensive measurement campaigns: the nucleation and cloud condensation nuclei (NCCN) study that was carried out in Atlanta, Georgia, during July and August 2009 (Jiang et al., 2011b), and a new particle formation and growth study carried out at the Foothill Laboratory of the National Center for Atmospheric Research (NCAR) in Boulder, Colorado, during August and September 2010. Geographic and meteorological conditions at the NCAR site are described in Zhao et al. (2010). Observations of significant particle production at 3 nm followed by rapid growth to potential CCN-active sizes (~80 nm diameter at 0.2 % supersaturation) have frequently been made at both sites during the summer (Stolzenburg et al., 2005; Kuang et al., 2009). While only a limited number of NPF events are presented in this study, their corresponding results are consistent with the results from other NPF events obtained during both campaigns.

In the NCCN study, freshly nucleated aerosol size distributions down to 1 nm geometric diameter were acquired with a newly developed scanning mobility particle spectrometer

(SMPS) utilizing a DEG UCPC as the particle detector (Iida et al., 2009; Jiang et al., 2011a). In this study, uncertainties in the measured size distribution arise from uncertainties in the chemistry-dependent activation efficiency of particles smaller than 2 nm geometric diameter using the DEG UCPC, uncertainties in the chemistry and size-dependent charging below 2 nm geometric diameter, and uncertainties from particle counting statistics in the DEG UCPC; uncertainties in the measured particle diameter were assumed to be negligible in comparison and were therefore not considered in this analysis. Further details regarding the setup and operation of the DEG SMPS are described in Jiang et al. (2011a). In the NCAR study, a DEG SMPS was also deployed and was operated identically to the system used in the NCCN study, except for the DEG UCPC, which was operated at a higher aerosol flow-rate and saturator temperature for increased particle detection efficiency (Kuang et al., 2012). Aerosol number size distributions at larger sizes were acquired with a conventional SMPS system (3 to 500 nm) (Woo et al., 2001) during NCCN and with a commercial TSI SMPS system (10 to 500 nm) during the NCAR campaign. A cluster chemical ionization mass spectrometer (Cluster CIMS) (Zhao et al., 2010) was also deployed during both campaigns to measure concentrations of gas-phase sulfuric acid monomer, [H_2SO_4], and neutral molecular clusters formed by nucleation. Systematic uncertainties in the measurement of [H_2SO_4] lead to an upper and lower limit that is a factor of 1.3 above and below the reported concentration, respectively; random relative uncertainties were assumed to be 10 % (Zhao et al., 2010; Jiang et al., 2011b). Further details regarding estimation of uncertainties in the measurement of [H_2SO_4] can be found in the appendices. During NCCN, direct measurements of the molecular composition of freshly nucleated 10 to 40 nm diameter particles were performed using a Thermal Desorption Chemical Ionization Mass Spectrometer (TDCIMS) (Smith et al., 2004). The TDCIMS measured particles with mobility diameters chosen to correspond to the peak of the growing nucleation mode. Molecular composition was inferred from the ion current detected in both positive and negative ion mass spectra, with uncertainties typically ranging from 10 to 30 % (Smith et al., 2008; Smith and Rathbone, 2008).

2.2 Data analysis

DEG SMPS raw data were inverted to yield aerosol number size distributions (Knutson, 1976; Stolzenburg and McMurry, 2008; Jiang et al., 2011a). While particles were size-classified according to their mobility diameter, results from this study are presented in terms of particle mobility diameter and particle geometric diameter, where the former is approximately 0.3 nm larger than the latter (Larriba et al., 2011). Estimated uncertainties in the measured size distribution and [H_2SO_4] were fully propagated in the subsequent analysis. Size and time-dependent observed particle growth

rates, GR_{OBS}, were estimated using two new methods based on fitting measured size distributions to the aerosol general dynamic equation (GDE) (Gelbard and Seinfeld, 1978). Whether the measured size distributions were consistent with sampling from a regional air mass or with interception of a local plume determined the appropriate method to obtain growth rates from the measured size distributions. The analysis method for plume events utilizes the novel result that size distributions ($< \sim 5$ nm) for a nucleating system in the presence of an aerosol achieve pseudo steady-state shortly after the start of nucleation (McMurry, 1983). For regional events, the analysis method is similar in principle to earlier analysis techniques (Lehtinen et al., 2004; Verheggen and Mozurkewich, 2006) that fit size distributions to the GDE. For an aerosol system that is growing through simultaneous gas uptake and coagulation, the aerosol GDE can be integrated to describe the evolution of the number concentration between particle diameters D_{p1} and D_{p2} ($D_{p2} > D_{p1}$) according to Eq. (1):

$$\frac{dN_\Delta(t)}{dt} = n(D_{p1}, t) \cdot GR(D_{p1}, t) - n(D_{p2}, t) \cdot GR(D_{p2}, t)$$
$$+ CoagSrc_\Delta(D_{p1}, D_{p2}, t) - CoagSnk_\Delta(D_{p1}, D_{p2}, t) \quad (1)$$

where Δ is the size interval defined by D_{p1} and D_{p2}, $GR = dD_p/dt$, and $n = dN/dD_p$. In the RHS of Eq. (1), the first and second terms are the condensational flux into and out of the aerosol size interval defined by Δ, $CoagSrc_\Delta$ is the source term defining the production of particles in Δ due to coagulation, and $CoagSnk_\Delta$ is the sink term defining the removal of particles in Δ due to coagulation. With a measured size distribution n, the only unknown quantities in Eq. (1) are the diameter growth rates at the interval boundaries, $GR(D_{p1}, t)$ and $GR(D_{p2}, t)$, which are then obtained as functions of time and particle diameter through an iterative solution of Eq. (1) at various particle sizes. Further details of each method can be found in Appendices A1 (regional event analysis) and A2 (plume event analysis). Previous methods for obtaining growth rates from size distributions typically require either a distinct nucleation mode (Mäkelä et al., 2000; Lehtinen and Kulmala, 2003; Stolzenburg et al., 2005) or a discernible time shift between concentration profiles at two sizes (Weber et al., 1997; Sihto et al., 2006). With the former method, it is not possible to analyze NPF events characterized by sustained periods of particle production as there is no distinct nucleation mode nor is it possible to de-couple the size and time-dependence of observed growth rates. With the latter method, NPF events with high growth rates are not amenable to analysis due to the potential lack of a discernible time shift, while growth rates that can be obtained are often averaged over large size intervals (1 to 6 nm) and time intervals (typically hours). Both methods used in this study were developed to exploit the strong size and time-dependence inherent in freshly nucleated aerosol size distribution measurements down to 1 nm without the restrictions of earlier methods.

Size and time-dependent particle growth rates due solely to the condensation of sulfuric acid, GR_{SA}, were calculated using measured sulfuric acid concentrations and assuming bulk properties for the sulfuric acid vapor (density $= 1.84\,g\,cm^{-3}$), explicitly accounting for the dimension and motion of collision partners during condensation (Fuchs, 1964; Lehtinen and Kulmala, 2003; Seinfeld and Pandis, 2006); the effects of interaction potentials were neglected. The size-dependent growth rate enhancement Γ (defined as the ratio of GR_{OBS} to GR_{SA}) was then obtained, quantifying the size-dependent contribution of species other than sulfuric acid to the observed growth. In this study, size-dependent particle growth rates GR_{OBS} and growth rate enhancements Γ down to 1 nm geometric diameter will be presented for a regional event measured during the NCAR campaign (19 September 2010) and for a plume event measured during NCCN (7 August 2009). The methods of analysis to obtain both $GR_{OBS}\left(D_p\right)$ and $\Gamma\left(D_p\right)$ for regional and plume events are described in Appendices 1.2 and 2.2, respectively. Based on the size-dependent growth rates and growth rate enhancements obtained for the events analyzed in this study, implications for nucleation and growth processes will be discussed, along with potential impacts on CCN production from new particle formation.

3 Results and discussion

3.1 Size-dependent growth rates

Observed size-dependent growth rates, $GR_{OBS}(D_p)$, down to 1 nm geometric diameter and their corresponding uncertainties are presented in Fig. 1a and b. Measurement uncertainties arising from particle counting statistics were included in the calculation of $GR_{OBS}(D_p)$. The effects of size-dependent uncertainties (in the composition dependent detection efficiency and in the bipolar charging efficiency) on $GR_{OBS}(D_p)$ are discussed in the appendices. The results in Fig. 1a are based on measurements in Atlanta on 7 August 2009 during the NCCN campaign. Growth rates increased systematically with size, and tended to be higher during the afternoon at 13:00 (5.5 ± 0.8 to $7.6 \pm 0.6\,nm\,h^{-1}$) than during the morning at 09:50 (2.1 ± 1 to $6.0 \pm 0.4\,nm\,h^{-1}$). These values of the growth rate are consistent with results reported in an earlier study at this site (Stolzenburg et al., 2005). We did not attempt to calculate growth rates for particles larger than 3 nm because the steady-state assumption required for analyzing size distributions from intercepted plumes becomes increasingly questionable as size increases (McMurry, 1983). The results in Fig. 1b are based on midday measurements at NCAR on 19 September 2010. Again, growth rates increased approximately linearly with size up to 3 nm geometric diameter during the period of peak particle production (13:00), increasing from $5.6 \pm 2\,nm\,h^{-1}$ to $27 \pm 5\,nm\,h^{-1}$ over the size range 0.8 to 3 nm geometric diameter. For the NCAR event,

growth rates were higher than were observed in Atlanta and were approximately constant with size for particles in the 3 to 5 nm geometric diameter size range. These high growth rates above 3 nm are comparable with those observed during intense periods of particle production and growth in Mexico City (Iida et al., 2008).

Previous studies have reported growth rate measurements during the initial steps of aerosol formation (Birmili et al., 2003; Kulmala et al., 2004b, c; Hirsikko et al., 2005; Stolzenburg et al., 2005; Iida et al., 2008; Manninen et al., 2009; Kuang et al., 2010), with some studies suggesting that diameter growth rates increase with size for the smallest particles (Kulmala et al., 2004b; Manninen et al., 2009). While those results were obtained from size distributions of the ambient ion population rather than from the total aerosol population (neutral and charged), such as reported here, their reported growth rate size-dependence is largely substantiated by our results in this study. The results from this study de-couple for the first time the size and time-dependence of observed particle growth rates, due to the new analysis methods which obtain size-dependent growth rates at a specified time. This de-coupling allows the clear interpretation of observed size-dependent growth to be an effect of the particle growth mechanism at work.

The size-dependence of the observed growth rates (up to ~ 3 nm geometric diameter for both analyzed events) can be compared with predictions of theoretical aerosol growth laws (Friedlander, 1977), providing information regarding possible mechanisms for aerosol growth. Particle growth laws that are qualitatively consistent with the observed increase in growth rate with size include: (1) nano-Köhler activation of nanometer-sized nuclei (Kulmala et al., 2004a), (2) multi-component diffusion corrected for the effect of particle curvature on vapor pressure (Kelvin effect), and (3) surface or volume-controlled reaction corrected for the Kelvin effect on surface and volume concentrations, respectively (Friedlander, 1977; Heisler and Friedlander, 1977; McMurry and Wilson, 1982; Kulmala et al., 2004b). The observed size-dependence could very well be a result of a combination of growth mechanisms occurring simultaneously.

3.2 Size-dependent growth rate enhancements

Size-dependent growth rate enhancements, $\Gamma(D_p)$, down to 1 nm geometric diameter and their corresponding uncertainties are presented in Fig. 2a and b. Measurement uncertainties arising from particle counting statistics and random error in the measurement of $[H_2SO_4]$ were included when calculating the uncertainties in $\Gamma(D_p)$. The effects of size-dependent uncertainties (in particle detection and charging efficiency) and systematic uncertainties in the measurement of $[H_2SO_4]$ are discussed in the appendices. The results in Fig. 2a are based on values of $GR_{OBS}(D_p)$ and $GR_{SA}(D_p)$ obtained during the morning at 09:50 and the afternoon at 13:00 for the NPF event measured on 7 August 2009
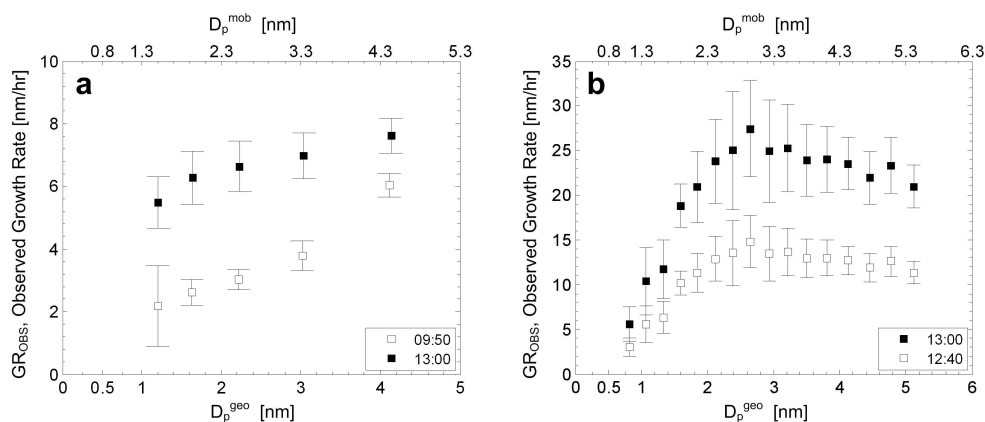
Fig. 1. Observed growth rates and corresponding uncertainties are plotted as functions of particle mobility diameter D_p^{mob} (upper abscissa) and geometric diameter D_p^{geo} (lower abscissa) for NPF events measured on **(a)** 7 August 2009 (NCCN), where uncertainties are presented as one standard deviation and on **(b)** 19 September 2010 (NCAR study), where uncertainties are presented as one standard error, calculated according to Cantrell (2008). Geometric particle diameters were estimated according to Larriba et al. (2011).
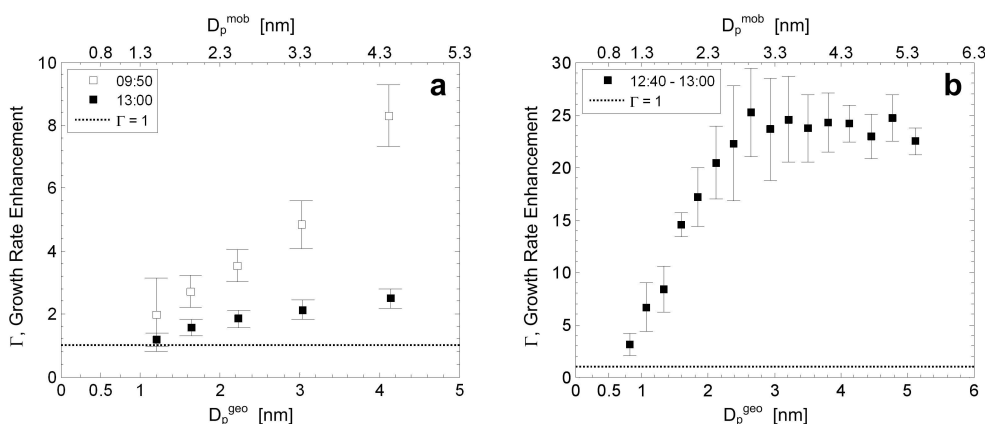

Fig. 2. Values of the growth rate enhancement Γ and their corresponding uncertainties are plotted as a function of particle mobility diameter D_p^{mob} (upper abscissa) and particle geometric diameter D_p^{geo} (lower abscissa) for the NPF event observed on **(a)** 7 August 2009 (NCCN), where uncertainties are presented as one standard deviation, and on **(b)** 19 September 2010 (NCAR) where uncertainties are presented as one standard error, calculated according to Cantrell (2008). A dotted line indicating $\Gamma = 1$ is shown for reference. Geometric particle diameters were estimated according to Larriba et al. (2011).

during the NCCN campaign. At 09:50, $\Gamma(D_p)$ increases with size, from 1.9 ± 1 at 1.2 nm geometric diameter, where sulfuric acid condensation accounts for ~50 % of the observed growth, to around 8.3 ± 1 at 4.1 nm geometric diameter, where sulfuric acid condensation accounts for ~10 % of the observed growth. During the afternoon at 13:00, a similar size-dependence for Γ was observed, albeit with lower values, ranging from 1.2 ± 0.2 at 1.2 nm geometric diameter, where sulfuric acid condensation accounts for nearly all the observed growth, to around 2.5 ± 0.3 at 4.1 nm geometric diameter, where sulfuric acid condensation accounts for ~40 % of the observed growth. These relatively low values of Γ are consistent with earlier observations in Atlanta of sulfuric acid-dominated condensational growth (Stolzenburg et

al., 2005; Kuang et al., 2010) and nanoparticles composed primarily of ammonium sulfate (Smith et al., 2005).

During 7 August 2009, the TDCIMS measured the composition of freshly nucleated particles at two sizes: 20 nm particles at the beginning of the NPF event (08:45–11:00), and 40 nm diameter particles later on during the event (13:30–14:30) in order to track the composition of the peak of the quickly growing nucleation mode. At the beginning of the event, measurements of the ion current indicated that dimethyl ammonium sulfate comprised ~3 % of the total molar composition of 20 nm diameter particles. Measurements of the composition of 40 nm particles later on during the event showed that sulfate salts of ammonium and dimethyl ammonium comprised ~60 % of the total molar composition.

TDCIMS measurements of freshly nucleated nanoparticle composition provide direct information of gas-phase species that participate in nanoparticle growth (Smith et al., 2008; Smith and Rathbone, 2008). The nanoparticle composition measurements on 7 August 2009 suggest that, at the beginning of the event, the observed growth rate for 20 nm particles is a factor of 30 higher than the corresponding sulfuric acid limited growth rate, which is consistent with the observation that nanoparticle composition is dominated by species other than sulfate. During the event, the TDCIMS measurements indicate that sulfate contributes an increasing amount to the composition of 40 nm particles, suggesting that the enhancement to growth is a factor of 1.5 for 40 nm particles. This observation of increasing sulfate contribution to nanoparticle composition (20 to 40 nm) measured by the TDCIMS supports the observed decrease in growth rate enhancement Γ (1 to 4 nm) from the morning to the afternoon measured by the DEG SMPS.

The results in Fig. 2b are obtained for the time interval 12:40–13:00 during the period of peak particle production for the NPF event measured on 19 September 2010 during the NCAR campaign. $\Gamma(D_p)$ increases approximately linearly with size during that time period, ranging from around 3.1 ± 1 at 0.8 nm geometric diameter, where sulfuric acid condensation accounts for $\sim$33 % of the observed growth (the balance of which could include volume contributions from associated ammonium and water), to 25 ± 4 at 2.7 nm geometric diameter, where sulfuric acid-limited condensation accounts for $\sim$5 % of the observed growth. Γ then remains approximately constant with size up to 5 nm geometric diameter. Values of Γ as high as 20 to 50 have been observed at other locations (Kuang et al., 2010). A number of studies have presented evidence of sulfuric acid limited condensation accounting for only a fraction of the observed sub 3 nm growth in ambient (Weber et al., 1997; Fiedler et al., 2005; Sihto et al., 2006) and laboratory experiments (Metzger et al., 2010). Due to the nature of the methods used to obtain sub 3 nm growth rates in those studies, the reported growth rate enhancements are, by definition, averages over the size and time it takes for a nucleated particle to grow to $\sim$3 nm. The growth rate enhancement values presented in Fig. 2a and b are the first reported results of size-resolved Γ down to $\sim$1 nm geometric diameter, providing a direct indication that species other than sulfuric acid can play a significant role in particle growth below 2 nm geometric diameter.

The values of Γ at the smallest particle sizes also provide insights into the nucleation process, namely, upper limit estimates on the critical cluster size. For both analyzed NPF events, Γ decreases with decreasing size, approaching values of 1.9 and 1.2 at 1.2 nm geometric diameter during the morning and afternoon of the NCCN event, respectively, and approaching a value of $\sim$3 at 0.8 nm geometric diameter during the period of particle production for the NCAR NPF event. It is worth noting that $GR_{SA}(D_p)$ is determined assuming zero evaporative flux of sulfuric acid from the particle sur-

face, leading to an upper limit estimate of $GR_{SA}(D_p)$ and, consequently, a lower limit estimate of Γ in this study. At the size of critical clusters or smaller, evaporation competes with or even overwhelms the sulfuric acid-limited condensation flux, and the resulting Γ is then substantially less than 1. Therefore, a Γ value greater than unity is only expected at sizes greater than the critical cluster size. For the NCCN event at 09:50, $\Gamma = 1.9$ at 1.2 nm geometric diameter, indicating that the critical cluster is formed at a smaller size, that the bottleneck to nucleation must occur below 1.2 nm geometric diameter. This result is consistent with the ambient aerosol size distribution measured at 10:00 (Jiang et al., 2011b), where the steepest drop in the distribution function occurs between [H_2SO_4] and [H_2SO_4]$_3$, implying that the bottleneck to nucleation occurs below $\sim$1 nm geometric diameter, the estimated size of the sulfuric acid trimer. For the NCAR event from 12:40–13:00, a Γ value of $\sim$3 suggests that the critical cluster size is less 0.8 nm geometric diameter.

3.3 Impact on nucleated particle survival probability

This observed size-dependence in growth rate up to 3 nm not only provides constraints on potential growth rate mechanisms, but also provides, for the first time, realistic growth rate inputs when modeling the nucleated particle survival probability in aerosol microphysical modules used in regional and chemical transport models (Pierce and Adams, 2007; Spracklen et al., 2008; Pierce and Adams, 2009; Wang and Penner, 2009; Spracklen et al., 2010). The nucleated particle survival probability is defined as the probability that a nucleated particle ($\sim$1 nm) will grow to a detectable size (3 nm) before being scavenged by the pre-existing aerosol. This probability is usually parameterized assuming a constant growth rate as the nucleated particles grow to 3 nm (Weber et al., 1997; Kerminen and Kulmala, 2002; McMurry et al., 2005; Lehtinen et al., 2007). Results from this study indicate that this assumption is not valid below 5 nm. The relative impact of a size-dependent growth rate on particle survival probability was modeled by numerically integrating the aerosol general dynamic equation for an aerosol population growing by simultaneous gas-uptake and coagulation (Friedlander, 1977; Gelbard and Seinfeld, 1978; Kuang et al., 2009), explicitly accounting for size-dependent growth below 3 nm. Measured inputs for this calculation were the observed size-dependent growth rates, growth rates derived from observed sulfuric acid concentrations, and the pre-existing aerosol size distribution obtained at 12:40 for the NCAR NPF event. Nucleated particle losses were determined exclusively from coagulation with the pre-existing aerosol. The results from this model calculation are event and environment-specific and are meant to be representative only of regions where sulfuric acid-limited condensation accounts for only a fraction of the observed growth. Model results for the survival probability as a function of final particle
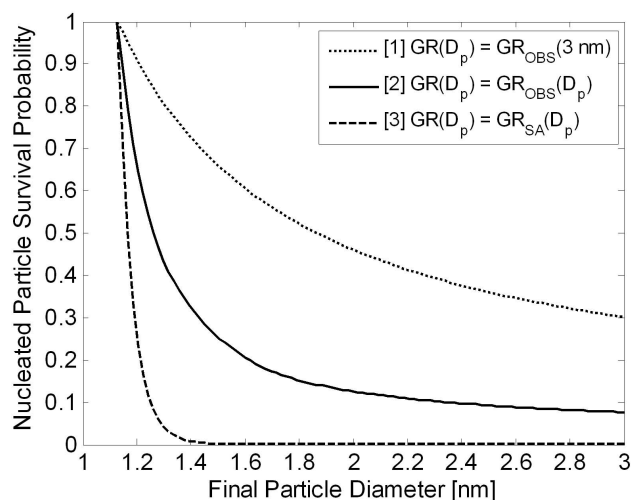
Fig. 3. Survival probability of a nucleated particle ($D_p = 1.12$ nm) as a function of final particle diameter for three growth rate scenarios: (1) $GR(D_p) = GR_{OBS}(3$ nm$)$, where the growth rate below 3 nm is assumed to be constant and equal to the observed growth at 3 nm (14 nm h^{-1}); (2) $GR(D_p) = GR_{OBS}(D_p)$, where the growth rate below 3 nm is equal to the observed size-dependent growth rate; and (3) $GR(D_p) = GR_{SA}(D_p)$, where the growth rate below 3 nm is equal to the size-dependent growth rate assuming the condensation of only sulfuric acid. Inputs for this model calculation were the observed size-dependent growth rates, growth rates derived from observed [H$_2$SO$_4$], and the pre-existing aerosol size distribution obtained at 12:40 for the NPF event on 19 September 2010 (NCAR).

size are shown in Fig. 3 for three growth rate scenarios: (1) constant growth – the growth rate below 3 nm is assumed to be constant and equal to the observed growth at 3 nm; (2) size-dependent growth – the growth rate below 3 nm is equal to the observed size-dependent growth rate; and (3) sulfuric acid-limited growth – the growth rate below 3 nm is equal to the size-dependent growth rate assuming only the condensation of sulfuric acid, a model for condensational growth that has been used in a number large-scale simulations (Pierce and Adams, 2007; Wang and Penner, 2009; Spracklen et al., 2010).

Under the size-dependent growth scenario, the modeled probability of a nucleated particle growing to 3 nm before being scavenged by the pre-existing aerosol is ∼8 %, orders of magnitude larger than the survival probability assuming sulfuric acid-limited growth, and ∼4× lower than the survival probability assuming a constant growth rate below 3 nm equal to the growth rate at 3 nm. While growth scenarios 1 and 3 have been regularly implemented in aerosol simulations, they can potentially lead to gross over and under-predictions of survival probability for particle growth to a CCN-active size, since particles are most vulnerable to loss below 3 nm. Accurate representation of the impact of NPF and growth on CCN production will require a mechanistic

understanding of the processes and species responsible for this size-dependent growth.

4 Summary

This study presents measurements and analysis methods that de-couple, for the first time, the size and time-dependence of diameter growth rates for freshly nucleated particles down to 1 nm geometric diameter. Data analysis methods were developed to obtain size-dependent growth rates at an instant in time for regional and plume NPF events by fitting the aerosol general dynamic equation to measured size distributions. Observed growth rates were found to increase approximately linearly with size from 1 to 3 nm geometric diameter, consistent with predictions from nano-Köhler theory, and Kelvin-limited diffusion, surface, and volume growth laws. Corresponding growth rate enhancements Γ were also found to increase approximately linearly with size, starting from ∼1 and 3 at the smallest sizes (1.2 and 0.8 nm geometric diameter, respectively) and reaching values as high as 8 and 25 (4.1 and 2.7 nm geometric diameter, respectively) for the events that were analyzed in this study. The contribution of species other than sulfuric acid to the observed growth for the analyzed events is significant below 3 nm, accounting for up to 95 % of the observed growth. For such events where growth is dominated by species other than sulfuric acid, neglecting size-dependent growth could lead to a significant overestimation of the resulting CCN survival probability. Further measurements and analyses of freshly nucleated aerosol number size distributions will help to provide further constraints and insights into ambient nucleation and growth processes, complementing measurements of particle composition by mass spectrometry.

Appendix A

Decoupling the size and time dependence of particle diameter growth rates

Data analysis methods were developed to obtain aerosol population dynamics information from measured size distributions, namely the aerosol diameter growth rate as a function of particle diameter and time during the period of particle production and growth. Two different approaches were used to obtain these growth rates, depending on whether the nucleation event was more regional or plume-like in nature.

A1 Regional event analysis

A1.1 Model development

For a regional event, the state of the aerosol system is characterized as being spatially and chemically homogeneous.

In such a system, the evolution of the number concentration between sizes D_{p1} and D_{p2} ($D_{p2} > D_{p1}$) for an aerosol system that is growing through simultaneous growth due to gas uptake and coagulation is described mathematically with the following population balance equation (Eq. A1) (Gelbard and Seinfeld, 1978) and term definitions (Eqs. A2–A4):

$$\frac{dN_\Delta(t)}{dt} = n(D_{p1}, t) \cdot GR(D_{p1}, t) - n(D_{p2}, t) \cdot GR(D_{p2}, t)$$
$$+ \text{CoagSrc}_\Delta(D_{p1}, D_{p2}, t) - \text{CoagSnk}_\Delta(D_{p1}, D_{p2}, t) \quad \text{(A1)}$$

$$\frac{dN_\Delta(t)}{dt} = \frac{d}{dt}\left(\int_{D_{p1}}^{D_{p2}} n(D_p, t) dD_p\right) \quad \text{(A2)}$$

$$\text{CoagSnk}_\Delta(D_{p1}, D_{p2}, t) = \int_{D_{p1}}^{D_{p2}} n(\overline{\overline{D_p}}, t) \cdot d\overline{\overline{D_p}}$$

$$\cdot \int_0^\infty \beta(\overline{\overline{D_p}}, \overline{D_p}) \cdot n(\overline{D_p}, t) \cdot d\overline{D_p} \quad \text{(A3)}$$

$$\text{CoagSrc}_\Delta(D_{p1}, D_{p2}, t) = \int_{D_{p1}}^{D_{p2}} \overline{\overline{D_p^2}} \cdot d\overline{\overline{D_p}}$$

$$\cdot \int_0^{\overline{\overline{D_p}}/2^{1/3}} \beta(\psi, \overline{D_p}) \cdot n(\psi, t) \cdot n(\overline{D_p}, t) \cdot \frac{d\overline{D_p}}{\psi^2} \quad \text{(A4)}$$

where Δ is the size interval defined by D_{p1} and D_{p2}, $GR = dD_p/dt$, $n = dN/dD_p$, β is the Fuchs form of the Brownian coagulation coefficient (Lehtinen and Kulmala, 2003; Seinfeld and Pandis, 2006), and $\psi^3 + \overline{D_p}^3 = \overline{\overline{D_p}}^3$. In the LHS of Eq. (A1), $\frac{dN_\Delta(t)}{dt}$ is the time rate of change of the size distribution n integrated from D_{p1} to D_{p2}. In the RHS of Eq. (A1), the first and second terms are the condensational flux into and out of the aerosol size interval defined by Δ, CoagSrc$_\Delta$ is the coagulation source term defining the production of particles in Δ due to the coagulation of particles, and CoagSnk$_\Delta$ is the coagulation sink term defining the removal of particles in Δ due to self-coagulation of particles within Δ, coagulation with particles smaller than D_{p1}, and coagulation with particles larger than D_{p2}. Equation (A1) is simply the general dynamic equation integrated from D_{p1} to D_{p2} (Gelbard and Seinfeld, 1978), where CoagSrc$_\Delta$ and CoagSnk$_\Delta$ define the total (rather than net) gain and loss, respectively, in particle number in Δ due to coagulation. With a measured size distribution n, the only unknown quantities in Eq. (A1) are the diameter growth rates at the interval boundaries, $GR(D_{p1}, t)$ and $GR(D_{p2}, t)$.

The condensational flux at D_{p1} is defined as (Heisler and Friedlander, 1977; Weber et al., 1996):

$$J_{\text{flux}}(D_{p1}, t) = n(D_{p1}, t) \cdot GR(D_{p1}, t). \quad \text{(A5)}$$

Equation (A1) can be re-arranged to yield an equivalent expression for the condensational flux at D_{p1}:

$$J_{\text{bal}}(D_{p1}, t) = \frac{dN_\Delta(t)}{dt} + n(D_{p2}, t) \cdot GR(D_{p2}, t) \quad \text{(A6)}$$
$$- \text{CoagSrc}_\Delta(D_{p1}, D_{p2}, t) + \text{CoagSnk}_\Delta(D_{p1}, D_{p2}, t)$$

where the subscript in J_{bal} refers to the balance method by which $J(D_{p1}, t)$ is obtained (Sihto et al., 2006; Riipinen et al., 2007). To facilitate the analysis, the observed diameter growth rate $GR(D_p, t)$ is represented as the product of two terms, as shown in Eq. (A7):

$$GR(D_p, t) = \Gamma(D_p) \cdot GR_{\text{SA}}(D_p, t) \quad \text{(A7)}$$

where $GR_{\text{SA}}(D_p, t)$ is the diameter growth rate based on the condensation of only sulfuric acid vapor, and $\Gamma(D_p)$ is the ratio of the observed growth rate $GR(D_p, t)$ to $GR_{\text{SA}}(D_p, t)$, an empirical factor that represents the contribution of other species and processes to the observed growth. Implicit in Eq. (A7) is the assumption that Γ is constant with time at a given size. For the short time interval during the NPF event analyzed with this method, this assumption will be verified in the subsequent section describing how $\Gamma(D_{p2})$ is calculated. Substituting Eq. (A7) into Eqs. (A5) and (A6), and letting $J_{\text{SA}}(D_{p1}, t) = n(D_{p1}, t) \cdot GR_{\text{SA}}(D_{p1}, t)$, yields:

$$J_{\text{flux}}(D_{p1}, t) = \Gamma(D_{p1}) \cdot J_{\text{SA}}(D_{p1}, t) \quad \text{(A8)}$$

$$J_{\text{bal}}(D_{p1}, t) = \frac{dN_\Delta(t)}{dt} + n(D_{p2}, t) \cdot \Gamma(D_{p2}) \cdot GR_{\text{SA}}(D_{p2}, t) \quad$$
$$- \text{CoagSrc}_\Delta(D_{p1}, D_{p2}, t) + \text{CoagSnk}_\Delta(D_{p1}, D_{p2}, t) \quad \text{(A9)}$$

Equating Eqs. (A8) and (A9) then yields:

$$J_{\text{bal}}(D_{p1}, t) = \Gamma(D_{p1}) \cdot J_{\text{SA}}(D_{p1}, t). \quad \text{(A10)}$$

Values of $J_{\text{SA}}(D_{p1}, t)$ and $J_{\text{bal}}(D_{p1}, t)$ are obtained from the measured size distribution and sulfuric acid concentration, where $GR_{\text{SA}}(D_{p1}, t)$ is calculated using the measured sulfuric acid concentration and a sulfuric acid monomer volume and diameter assuming a bulk density of $1.84\,\text{g cm}^{-3}$.

Estimated uncertainties from the measurement of aerosol and sulfuric acid number concentrations are included and propagated through Eqs. (A1) through (A9). Correlations between individual terms in Eq. (A9) are included in the uncertainty propagation. For the results presented in the main text, uncertainties in the aerosol size distribution and number concentration are estimated from particle counting statistics (where it has been assumed that there is no uncertainty in the measurement of particle diameter), while random relative uncertainties in the measurement of [H$_2$SO$_4$] were assumed to be 10 %. The effects of systematic uncertainties in the measurement of [H$_2$SO$_4$] (see Appendix B) and the aerosol size distribution (due to uncertainties in chemistry-dependent detection efficiencies and charging efficiencies) are detailed in Appendix C.

With values of $\Gamma(D_{p2})$, obtained by a method which will be discussed in the subsequent section, a linear least-squares regression can be performed where values of $J_{bal}(D_{p1},t)$, $J_{SA}(D_{p1},t)$, and their corresponding uncertainties are fit to Eq. (A10), yielding a best-fit estimate for $\Gamma(D_{p1})$ and its standard error. Standard techniques for applying a least-squares algorithm to data with uncertainties in both coordinates were applied (Williamson, 1968; Neri et al., 1989; Cantrell, 2008). The time interval for this procedure is chosen to be long enough to yield a large enough data set for fitting ($\sim$20 min, 5 data points), but short enough so that the assumption of constant Γ over that brief time interval can be reasonably made. Fixing the upper size boundary at D_{p2} ($D_{p2} = 5.4$ nm), this regression procedure can then be repeated at different values of D_{p1} to obtain Γ as a function of size below D_{p2}.

A1.2 Determining Γ at the upper size boundary D_{p2}

Over a single size bin i ($\sim$0.5 nm bin spacing at $D_{p2} = 5.4$ nm geometric diameter), Eq. (A1) can be rewritten as:

$$\frac{dN_\Delta(t)}{dt} = \Gamma(i) \cdot J_{SA}(D_{p1},t) - \Gamma(i) \cdot J_{SA}(D_{p2},t)$$
$$+ CoagSrc_\Delta(D_{p1},D_{p2},t) - CoagSnk_\Delta(D_{p1},D_{p2},t) \quad \text{(A11)}$$

where Γ is initially assumed constant over such a small Δ bounded by D_{p1} and D_{p2}. This assumption will be relaxed during a subsequent iterative calculation of Γ. Re-arranging Eq. (A11) yields:

$$A(t) = \Gamma \cdot B(t) \quad \text{(A12)}$$

where A and B are defined as:

$$A(t) = \frac{dN_\Delta(t)}{dt} - CoagSrc_\Delta(D_{p1},D_{p2},t)$$
$$+ CoagSnk_\Delta(D_{p1},D_{p2},t) \quad \text{(A13)}$$

and

$$B(t) = J_{SA}(D_{p1},t) - J_{SA}(D_{p2},t). \quad \text{(A14)}$$

Values of A and B are calculated from the measured size distribution with corresponding uncertainties due to propagation of measurement uncertainties in aerosol and sulfuric acid number concentration. Correlations between terms in Eq. (A13) and between terms in Eq. (A14) are included in the uncertainty propagation. Values of A and B along with their uncertainties are then fit to Eq. (A12) to yield a best-fit estimate for $\Gamma(i)$ and its standard error using established methods (Williamson, 1968; Neri et al., 1989; Cantrell, 2008). The standard error is equal to the square root of the variance multiplied by the sum of squared residuals weighted by the inverse variances of the individual data points (Cantrell, 2008). An example of such a fit is shown in Fig. A1. The time interval selected for analysis in Fig. A1 corresponds to
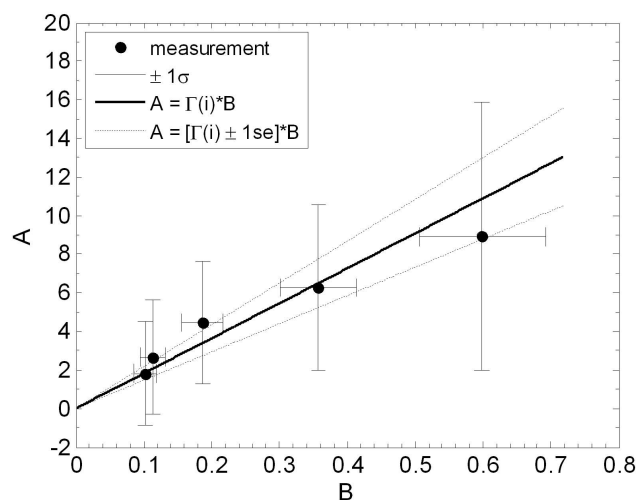

Fig. A1. Comparison of A and B calculated at 5.4 nm geometric diameter with a least-squares fit line over the time period 12:40–13:00 during an NPF event observed on 19 September 2010 in Boulder, CO (NCAR). A relative uncertainty of 10 % was assumed for the sulfuric acid concentration measurements when calculating B and its corresponding uncertainty. Median values of $[H_2SO_4]$ were used in this particular calculation (no systematic uncertainty applied). Uncertainties in A and B are presented as one standard deviation (1σ). The uncertainty in the best-fit value of Γ is presented as one standard error (1se) calculated according to Cantrell (2008).

a period of strong nucleation and rapid growth during the analyzed NPF event, where there are sufficient particle counts at the smallest bin sizes.

This initial best-fit estimate of $\Gamma(i)$ is then input into Eq. (A10) to determine $\Gamma(i-1)$ for the adjacent size bin. Relaxing the assumption of constant $\Gamma(i)$ over bin i in Eq. (A11), a weighting factor is then introduced into Eq. (A14) in order to match condensational fluxes at the boundary between bins i and $i-1$, yielding:

$$B(t) = \left(\frac{\Gamma(i) + \Gamma(i-1)}{2 \cdot \Gamma(i)}\right) \cdot J_{SA}(D_{p1},t) - J_{SA}(D_{p2},t). \quad \text{(A15)}$$

The subsequent calculation of a new $\Gamma(i)$ and $\Gamma(i-1)$ is iterated until $\Gamma(i)$ changes by less than a user-set criterion, in this case, 1 %. An example of this iterative convergence is shown in Fig. A2, where $\Gamma(i)$ at the upper boundary converges to a value of 18 ± 3.5 (one standard error). For this particular calculation, median values of $[H_2SO_4]$ were used (no systematic uncertainty applied). It should be noted that over a different time interval of similar length, $\Gamma(i)$ will likely be a different value.

A1.3 Determining $\Gamma(D_p)$ and $GR(D_p,t)$

As mentioned earlier, this converged, best-fit $\Gamma(D_{p2})$ and corresponding standard error is then used in Eqs. (A9) and (A10) to calculate best-fit $\Gamma(D_p)$ at sizes below D_{p2}, results
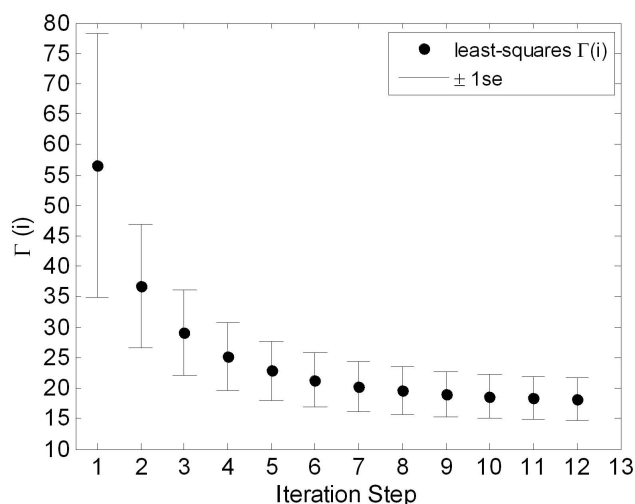
Fig. A2. Convergence of $\Gamma(i)$ as a function of iteration step. Values of A and B were calculated at 5.4 nm geometric diameter for the time period 12:40–13:00 during an NPF event observed on 19 September 2010 in Boulder, CO (NCAR). At each step, $\Gamma(i)$ and its corresponding standard error (1se) were obtained by a linear least-squares fitting method modified for regression through the origin with measurement uncertainties in both axes (Cantrell, 2008). Median values of $[H_2SO_4]$ were used in this particular calculation (no systematic uncertainty applied).

Fig. A3. Time-dependent particle number concentrations at various particle geometric diameters D_p for collision-controlled nucleation in the free-molecular regime for a system that is initially particle-free. For particles smaller than 5 nm, less than an hour is needed to reach a quasi-steady state. After quasi-steady state is reached, the decrease in number concentration is due to the increase of aerosol surface area (a coagulation sink), and does not depend explicitly on time.

of which are shown in the main text in Fig. 2b. Using Eq. (A7) and best-fit estimates of $\Gamma(D_p)$, the observed growth rates $GR_{OBS}(D_p)$ and resulting uncertainties can be calculated, results of which are shown in the main text in Fig. 1b.

A2 Plume event analysis

A2.1 Steady state assumption

Previous work has shown that in a nucleating system, steady state concentrations can be achieved for small particles (∼5 nm) in time periods of less than about one hour for typical atmospheric conditions (McMurry, 1983). This steady state is due to the balance between formation from smaller particles by condensation and coagulation, and removal by coagulation with particles of all sizes. Figure A3 shows the simulation results for collision-controlled nucleation in a system that initially contains no particles and with the monomer concentration fixed at 1×10^8 #cm^{-3}, which is in the range of sulfuric acid vapor concentrations observed in Atlanta during NCCN 2009. Concentrations initially increase rapidly because formation rates exceed coagulation loss rates due to the low particle concentrations immediately following formation. After 30 to 60 min, however, quasi-steady state is achieved. The slow, steady decrease in concentrations with time (t) that is observed after this period is due to the gradual increase in coagulation losses resulting from the increas-
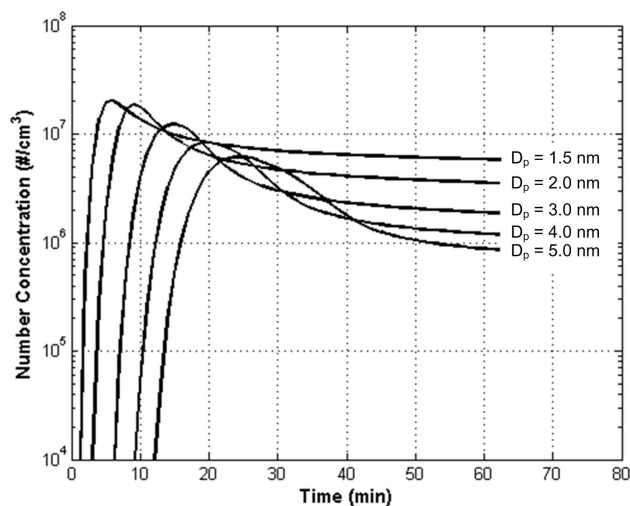
ing aerosol surface area.as time progresses. For free molecular kinetics, which was assumed in obtaining these illustrative results, coagulation losses vary in proportion to the pre-existing aerosol surface area, which varies in proportion to $t^{1/5}$ (McMurry and Friedlander, 1977). Although the time dependence for atmospheric aerosols (which fall in the transition regime) will have a quantitatively different time dependence, it will follow a qualitatively similar weak dependence on time. It is this weak time dependence that allows the establishment of a quasi-steady-state determined by the instantaneous aerosol size distribution.

All the new particle formation events observed in Atlanta during the 2009 intensive measurement campaign appear to be due to the impact of plumes from nearby coal-fired power plants. Evidence for this is the correlation between concentrations of freshly nucleated particles and $[SO_2]$, and the sharp variabilities in particle concentrations as the wind transported the plume towards and away from our site. We estimate that, depending on the wind direction and speed, transport times from the stack to the sampling site typically exceeded about two hours. This leads us to conclude that number distribution functions of sub − 5 nm particles should be quasi-steady-state.

A2.2 Model development

For each 15 min measurement of the aerosol size distribution, a smooth curve is fitted to obtain a continuous size distribution. Number distributions were obtained by merging

data from the Cluster Chemical Ionization Mass Spectrometer (Cluster CIMS) and a diethylene glycol scanning mobility sizing spectrometer (DEG SMPS) data as described by Jiang et al. (2011b) and shown in Fig. A4. The fit to the measured size distribution was performed for sizes ranging from 0.8 nm geometric diameter (clusters containing 3 sulfuric acid molecules) to 5.0 nm geometric diameter. Particle geometric diameters were estimated from measured mobility diameters according to the method of Larriba et al. (2011). Applying steady state to the number concentration in the GDE of Eq. (A1) (Appendix A.1.1) yields:

$$0 = n(D_{p1}, t) \cdot \mathrm{GR}(D_{p1}, t) - n(D_{p2}, t) \cdot \mathrm{GR}(D_{p2}, t)$$
$$+ \mathrm{CoagSrc}_\Delta(D_{p1}, D_{p2}, t) - \mathrm{CoagSnk}_\Delta(D_{p1}, D_{p2}, t) \quad \text{(A16)}$$

where the terms $\mathrm{CoagSnk}_\Delta$ and $\mathrm{CoagSrc}_\Delta$ are defined in Eqs. (A3) and (A4), respectively, $n = dN/dD_p$, and GR is the particle diameter growth rate. In the plume analysis method, D_{p1} and D_{p2} are adjacent size bins. GR is estimated by first solving Eq. (A16) for GR through iteration, initially assuming $\mathrm{GR}(D_{p1}, t) = \mathrm{GR}(D_{p2}, t)$. This is a reasonable starting point provided that the diameter bin sizes dD_p are small enough. So for each size D_{p1} we first obtain $\overline{\mathrm{GR}(D_{p1}, t)}$, defined by:

$$\overline{\mathrm{GR}(D_{p1}, t)} = \quad \text{(A17)}$$
$$-\frac{\mathrm{CoagSrc}_\Delta(D_{p1}, D_{p2}, t) - \mathrm{CoagSnk}_\Delta(D_{p1}, D_{p2}, t)}{n(D_{p1}, t) - n(D_{p2}, t)}.$$

For subsequent iterations,

$$\mathrm{GR}(D_{p1}, t) \cong \quad \text{(A18)}$$
$$-\frac{\mathrm{CoagSrc}_\Delta(D_{p1}, D_{p2}, t) - \mathrm{CoagSnk}_\Delta(D_{p1}, D_{p2}, t)}{n(D_{p1}, t) - n(D_{p2}, t) \cdot \frac{\overline{\mathrm{GR}(D_{p2}, t)}}{\overline{\mathrm{GR}(D_{p1}, t)}}}.$$

The relative change in $\mathrm{GR}(D_{p1}, t)$ after one iteration is less than 3 %.

A2.3 Calculation of the relative uncertainty

Uncertainties in the number concentration N and the diameter growth rate GR are estimated at each size for which measurements were obtained.

Uncertainties in N

The particle concentration N for each size bin is calculated using Eq. (A19):

$$N = \frac{C}{\eta_t f_{\mathrm{detection}} f_{\mathrm{charging}} Q_a} \quad \text{(A19)}$$

where C is the number of particles counted by the DEG UCPC, $f_{\mathrm{detection}}$ is the size-dependent DEG detection efficiency (which includes the activation efficiency and fractional diffusional deposition), f_{charging} is the size-dependent
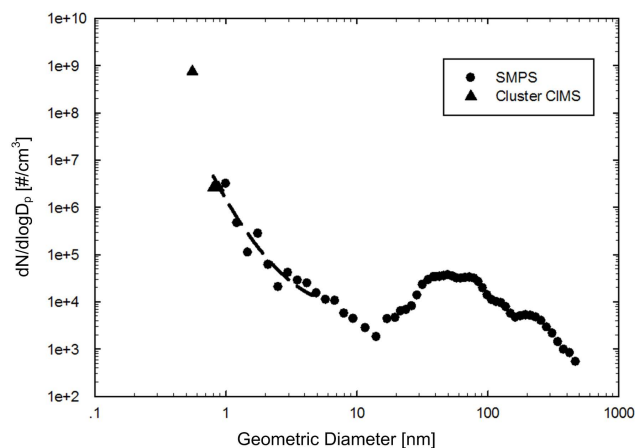

Fig. A4. Particle size distribution observed on 13:00, 7 August 2009 (NCCN). Filled triangles are data obtained by the cluster chemical ionization mass spectrometer (Cluster CIMS) and filled circles are data obtained from two scanning mobility particle spectrometers (SMPS) (Jiang et al., 2011b). The dashed line is obtained by fitting a second order polynomial using the method of least squares to the data over the size range where growth rates are calculated in this work.

charged fraction, Q_a is the aerosol flow rate through the DEG UCPC, and η_t is the size and flow rate-dependent particle transmission efficiency through the sampling system upstream of the DEG UCPC. The relative uncertainty for C is $1/\sqrt{C}$, which is derived by assuming particle counting as a Poisson process. Flow rates were calibrated twice daily and were accurate to within 5 %. Uncertainties in flow rate (and η_t) are therefore negligible relative to other uncertainties. Wiedensohler's approximation for Fuchs' diffusion charging theory (Wiedensohler, 1988) is used to calculate the charging fraction f_{charging}. Since the charged fraction for particles smaller than 2 nm has not been studied, relative uncertainties in f_{charging} are difficult to quantify and have been neglected in this section. However, the effects of uncertainties in f_{charging} on the inverted size distributions and subsequent growth rate calculations can be determined and are investigated in Appendix C. The relative uncertainty for $f_{\mathrm{detection}}$ is determined from the activation efficiency of sodium chloride particles (Jiang et al., 2011a). If activation efficiencies of freshly nucleated atmospheric particles are different from sodium chloride, this will lead to systematic errors in the inverted size distribution, which have been neglected in this section. The effects of uncertainties in activation efficiency on the inverted size distributions and growth rate calculations are investigated in Appendix C. With these assumptions, the relative error for N is,

$$\frac{\Delta N}{N} = \frac{\sqrt{\left(\frac{\partial N}{\partial C}\right)^2 \Delta C^2 + \left(\frac{\partial N}{\partial \eta_{\text{detection}}}\right)^2 \Delta \eta_{\text{detection}}^2}}{N}$$

$$= \sqrt{\frac{1}{C} + \left(\frac{\Delta \eta_{\text{detection}}}{\eta_{\text{detection}}}\right)^2}. \tag{A20}$$

Uncertainties in GR

Uncertainties in the size of mobility-classified particles are negligible relative to uncertainties in number concentration and are therefore neglected in this analysis. Let Eq. (A17) be rewritten:

$$\text{GR}(D_{\text{p1}}, t) = -\frac{A}{B} \tag{A21}$$

where $A = \text{CoagSrc}_\Delta(D_{\text{p1}}, D_{\text{p2}}, t) - \text{CoagSnk}_\Delta(D_{\text{p1}}, D_{\text{p2}}, t)$ and $B = n(D_{\text{p1}}, t) - n(D_{\text{p2}}, t)$.

For the sub − 5 nm particles of interest in this study, the relative uncertainty in A is approximately $\Delta N/N$. For B, $n(D_{\text{p1}}, t)$ and $n(D_{\text{p2}}, t)$ are highly correlated when the bin size is small. The correlation coefficient ρ between $n(D_{\text{p1}}, t)$ and $n(D_{\text{p2}}, t)$ is larger than 0.997 for the data sets we use. The relative uncertainty in B can be expressed as,

$$\frac{\Delta B}{B} = \tag{A22}$$

$$\frac{\sqrt{(\Delta n(D_{\text{p1}}, t))^2 + (\Delta n(D_{\text{p2}}, t))^2 - 2\rho \Delta n(D_{\text{p1}}, t) \Delta n(D_{\text{p2}}, t)}}{B}$$

$$\approx \frac{\Delta N}{N}.$$

The relative uncertainty of GR is then,

$$\frac{\Delta \text{GR}}{\text{GR}} = \sqrt{\left(\frac{\Delta A}{A}\right)^2 + \left(\frac{\Delta B}{B}\right)^2 - 2\rho_{AB} \frac{\Delta A \Delta B}{AB}} \tag{A23}$$

where ρ_{AB}, the correlation coefficient between A and B, is estimated from measurements of the whole day and is found to have a value between 0.2 and 0.3.

Uncertainties in the growth rate enhancement Γ

The growth rate enhancement Γ is defined as the ratio of the observed growth rate to the growth rate due to condensation of sulfuric acid only:

$$\Gamma = \frac{\text{GR}}{\text{GR}_{\text{SA}}} \sim \frac{\text{GR}}{[\text{H}_2\text{SO}_4]} \tag{A24}$$

with a relative uncertainty defined as:

$$\frac{\Delta \Gamma}{\Gamma} = \sqrt{\left(\frac{\Delta \text{GR}}{\text{GR}}\right)^2 + \left(\frac{\Delta [\text{H}_2\text{SO}_4]}{[\text{H}_2\text{SO}_4]}\right)^2}. \tag{A25}$$

In this calculation, a relative random uncertainty of ±10 % was assumed for $[\text{H}_2\text{SO}_4]$. The effects of systematic uncertainties in $[\text{H}_2\text{SO}_4]$ on the calculation of Γ are discussed in Appendix C1.

Appendix B

Estimation of systematic uncertainties in the measurement of [H₂SO₄] using the Cluster CIMS

Sulfuric acid concentration ([SA]) was calculated according to the following equation (Berresheim et al., 2000):

$$[\text{SA}] = cf_{\text{m}} \frac{1}{kt} \ln\left(1 + \frac{S_{\text{SA}}}{S_{\text{Re}}}\right) \tag{B1}$$

where cf_{m} is the mass-dependent transmission factor, k is the ion-molecular rate constant, t is the measured reaction time, S_{SA} is the counting rate for sulfuric acid summing over m/z 97 (when available) and 160, and S_{Re} is the counting rate for the reagent ions summing over m/z 125 and 188. The overall systematic uncertainty in [SA] can be estimated from the systematic uncertainties in each term of Eq. (B1). The uncertainty associated with the ion-molecular rate constant k was obtained from the measurements of Viggiano et al. (1997), who estimated a relative systematic uncertainty of ±10 to 15 %. Here, we use a value of $k = 1.86 \times 10^{-9}$ cm³ s⁻¹, the rate constant between sulfuric acid and the reagent ion $\text{NO}_3^- \text{HNO}_3$, assuming it is the predominant reagent ion. However, concentrations of $\text{NO}_3^- (\text{HNO}_3)_2$ are sometimes elevated, which introduces an additional uncertainty. Therefore, a slightly higher relative systematic uncertainty of ±20 % is used in this analysis. The relative uncertainty associated with the ratio $S_{\text{SA}}/S_{\text{Re}}$ was estimated to be ±10 % from laboratory measurements with relatively stable sulfuric acid concentrations. For ambient measurements, the relative uncertainty is expected to be somewhat larger, ±15 %. Background measurements (usually taken at night) have a counting rate lower than 100 Hz, which is equal to about 2×10^5 cm⁻³. Given that sulfuric acid concentrations during an NPF event are above 10^6 cm⁻³, background counts have a negligible impact on the calculation of sulfuric acid concentration. The relative systematic uncertainty associated with the ratio $S_{\text{SA}}/S_{\text{Re}}$ is therefore estimated to be about ±15 %. The relative systematic uncertainty associated with the mass-dependent transmission factor cf_{m} was estimated to be ±10 % for the Cluster CIMS using positive ions (Zhao et al., 2010), and is a combination of the transmission efficiency through the octopole and quadrupole, and the mass discrimination of the electron multiplier. Values for the reaction time t were measured, yielding a relative systematic uncertainty of ±10 %. Propagating the uncertainties in the individual terms in Eq. (B1) yields an overall relative systematic uncertainty of ±30 % for the measurement of [SA].
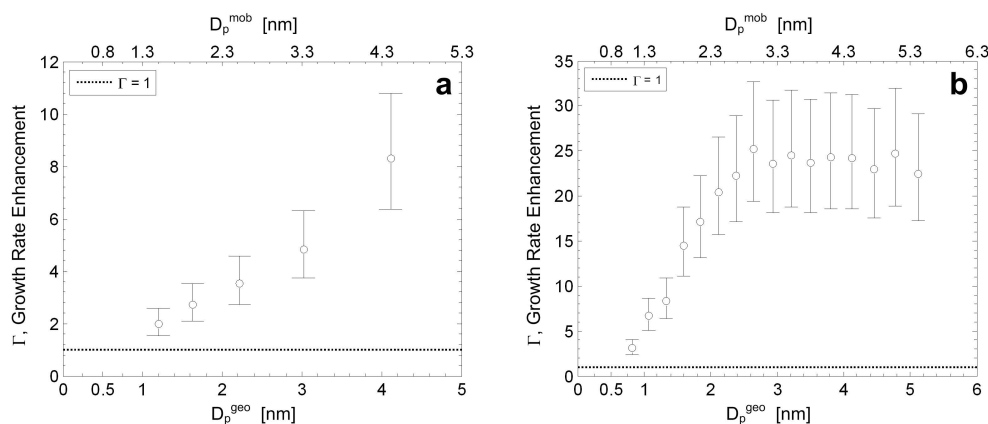
Fig. B1. Effect of systematic uncertainties in [H_2SO_4] on growth rate enhancement Γ as a function of particle mobility diameter D_p^{mob} (upper abscissa) and particle geometric diameter D_p^{geo} (lower abscissa) for the NPF event observed on **(a)** 7 August 2009 (09:50, NCCN) and on **(b)** 19 September 2010 (12:40–13:00, NCAR). Values of Γ calculated using the median values of [H_2SO_4] are presented as open circles. Resulting upper and lower limits on Γ, based on lower and upper limits on [H_2SO_4] known to within a factor of 1.3, are shown for each value of Γ as horizontal bars. A line indicating $\Gamma = 1$ is shown for reference. Geometric particle diameters were estimated according to Larriba et al. (2011).

Appendix C

Effect of systematic measurement uncertainties on Γ

C1 Effect of systematic uncertainties in the measurement of [H_2SO_4]

A systematic relative uncertainty of $\pm 30\%$ for the Cluster CIMS measurement of [H_2SO_4] leads to upper and lower limits that are a factor of 1.3 above and below the reported concentrations. The effect of this systematic uncertainty was propagated through the relevant equations in Appendix A, the results of which are shown in Fig. C1a for the NCCN event and in Fig. C1b for the NCAR event. The only effect of this systematic uncertainty in [H_2SO_4] is to either increase or decrease the sulfuric acid-limited growth rate GR_{SA} and the resulting $\Gamma(D_p)$ by a factor of 1.3 at each size D_p (see Eqs. A7 and A24). While the range between values of $\Gamma(D_p)$ is somewhat large (1.7×), the dependence of Γ on size is unambiguous since the applied uncertainty is systematic. There is no effect on the observed growth rate $GR_{OBS}(D_p)$ since the calculation of $GR_{OBS}(D_p)$ does not depend on [H_2SO_4].

C2 Effect of systematic uncertainties in chemistry-dependent parameters: size-dependent charging efficiency and DEG UCPC detection efficiency

C2.1 NCCN event

In this study, the number concentrations of mobility-classified particles are calculated according to the equation (see Appendix A.2.3.1 for the description of individual terms):

$$N = \frac{C}{\eta_t \, f_{detection} \, f_{charging} \, Q_a}. \tag{C1}$$

We believe the primary sources of uncertainty in calculated values of N are associated with uncertainties in $f_{detection}$ and $f_{charging}$, both of which become more uncertain as particle size decreases and may depend on composition (O'Dowd et al., 2002; Iida et al., 2009; Jiang et al., 2011a; Premnath et al., 2011). We have measured $f_{detection}$ in the laboratory for particles of known composition (NaCl, Ag, and tetra-alkyl ammonium ions $N^+[C_nH_{2n+1}]_4$). For the salt and metals, measurements were done for particles of different charges: $+1$, 0, and -1. Some of these data were reported by Jiang et al. (2011a), and more results will be described in forthcoming publications. The DEG UCPC did not detect Ag particles smaller than 1.7 nm mobility diameter, while atmospheric nuclei as small as 1.1 nm mobility diameter were detected. The tetra-alkyl ammonium ions were even more difficult to detect than the silver. Furthermore, we found that if $f_{detection}$ is assumed equal to values measured for sodium chloride and $f_{charging}$ is calculated using bipolar stationary state theory (Wiedensohler, 1988; Reischl et al., 1996; Alonso et al., 1997), distribution functions measured with the DEG SMPS are in good qualitative agreement with distribution functions of neutral molecular clusters measured independently by the cluster chemical ionization mass spectrometer (Cluster CIMS) (Jiang et al., 2011b). Therefore, this is the approach that was used to calculate distribution functions in this study.

To estimate the effects of size-dependent uncertainties of the product $f_{detection} \cdot f_{charging}$, we assume that uncertainties increase linearly with decreasing size from $\pm 10\%$ at 3 nm
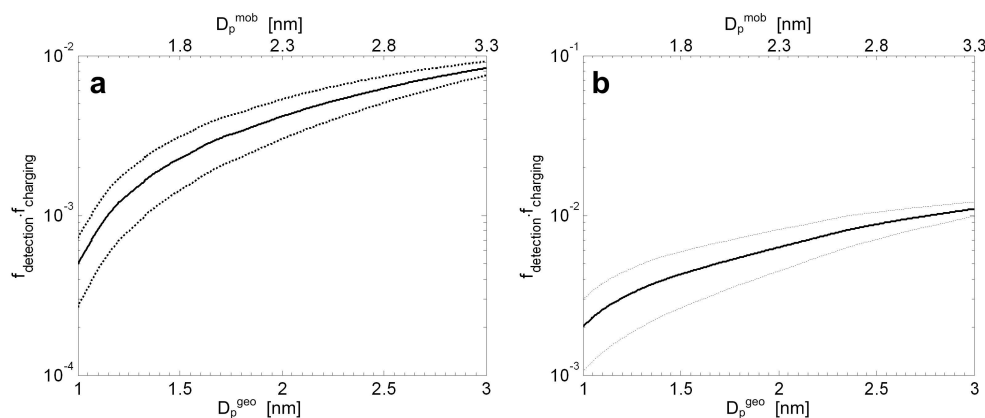
Fig. C1. Upper and lower bound estimates (dotted lines) to the quantity $f_{\text{detection}} \cdot f_{\text{charging}}$ (the product of size-dependent detection and charging efficiencies) as a function of particle mobility diameter $D_{\text{p}}^{\text{mob}}$ (upper abscissa) and particle geometric diameter $D_{\text{p}}^{\text{geo}}$ (lower abscissa) obtained for DEG SMPS operation during **(a)** NCCN and **(b)** the NCAR campaign. The differences between the two figures arise from differences in the detection efficiency: the DEG UCPC was operated at higher flow rates and super-saturation ratios during the NCAR study. For both campaigns, the same size-dependent systematic relative uncertainty in $f_{\text{detection}} \cdot f_{\text{charging}}$ was assumed, linearly decreasing from $\pm 50\%$ at 1 nm geometric diameter to $\pm 10\%$ at 3 nm geometric diameter. The solid black line represents the product of the size-dependent detection efficiency of negatively charged NaCl and the bipolar charging efficiency using the parameterization of Wiedensohler (1988). Geometric particle diameters were estimated according to Larriba et al. (2011).
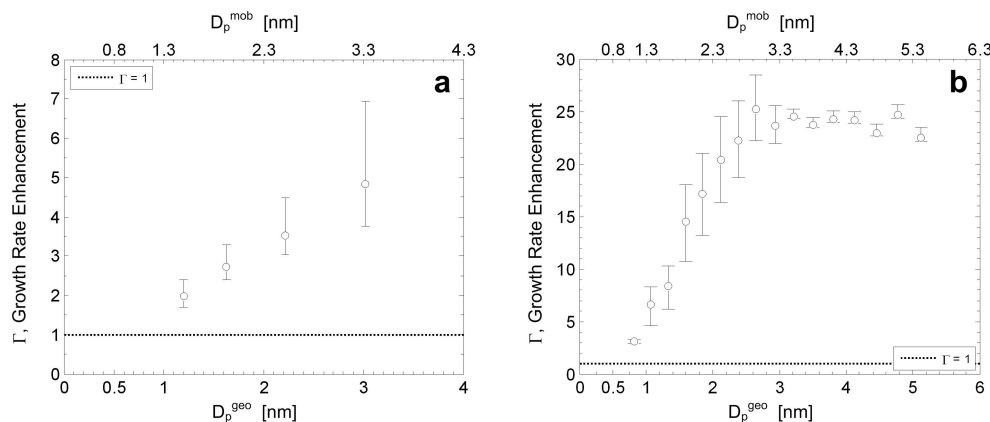

Fig. C2. Effects of systematic uncertainties in particle detection and charging efficiencies on growth rate enhancement Γ as a function of particle mobility diameter $D_{\text{p}}^{\text{mob}}$ (upper abscissa) and particle geometric diameter $D_{\text{p}}^{\text{geo}}$ (lower abscissa) for the NPF event observed on **(a)** 7 August 2009 (09:50, NCCN) and on **(b)** 19 September 2010 (12:40–13:00, NCAR). Values of Γ calculated using the size-dependent detection efficiency of negatively charged NaCl and the bipolar charging efficiency using the parameterization of Wiedensohler (1988) are presented as open circles. Resulting upper and lower limits on Γ, based on assumed systematic uncertainties in the product $f_{\text{detection}} \cdot f_{\text{charging}}$, are shown for each value of Γ as horizontal bars. A line indicating $\Gamma = 1$ is shown for reference. Geometric particle diameters were estimated according to Larriba et al. (2011).

to $\pm 50\%$ at 1 nm, as shown in Fig. C2a. The solid black line corresponds to the value of $f_{\text{detection}} \cdot f_{\text{charging}}$ used in our work, and the dotted lines show our upper and lower bounds for this product. We further assume that uncertainties of the same magnitude are associated with Cluster CIMS measurements of neutral molecular clusters that contained three or four sulfuric acid molecules. With these assumptions for systematic uncertainties in $f_{\text{detection}} \cdot f_{\text{charging}}$, upper and lower limits on the size-dependent growth rate enhancement factors, Γ, are calculated according the procedure described in

Appendix A2. Figure C3a shows the corresponding range of Γ for measurements at 09:50 on 7 August 2009. The relative uncertainty in Γ is about 15 % at 1.2 nm geometric diameter and 40 % at 3 nm geometric diameter. Furthermore, Γ approaches a value of unity close to 1 nm geometric diameter, and increases monotonically with size above that. It follows that our important qualitative conclusions, that Γ approaches unity for the smallest particles and increases systematically with size above that, are not seriously compromised by uncertainties in $f_{\text{detection}} \cdot f_{\text{charging}}$. The relative

effect of these same uncertainties on GR is identical to the effect on Γ since GR scales linearly with Γ according to Eq. (A7) ($GR = \Gamma \cdot GR_{SA}$) in the appendices, where GR_{SA} is the growth rate based on the condensation of only H_2SO_4 vapor.

C2.2 NCAR event

A similar calculation was performed for the NCAR event assuming the size-dependent product $f_{detection} \cdot f_{charging}$ presented in Fig. C2b, which has a slightly higher value compared to that used for the NCCN event, due to the higher values of $f_{detection}$ resulting from operating the NCAR DEG UCPC at a higher flow rate and instrument super-saturation compared to the NCCN DEG UCPC. For the NCAR event, a size-dependent systematic uncertainty in $f_{detection} \cdot f_{charging}$ was assumed, linearly decreasing from $\pm 50\%$ at 1 nm to $\pm 10\%$ at 3 nm. The resulting range in Γ due to this assumed systematic uncertainty in $f_{detection} \cdot f_{charging}$ is presented in Fig. C3b, where the upper and lower limits in Γ are still seen to increase monotonically with size up to $\sim$3 nm geometric diameter. The overall trends in $\Gamma(D_p)$ and the resultant conclusions are maintained given the prescribed systematic uncertainty in $f_{detection} \cdot f_{charging}$.

References

Alonso, M., Kousaka, Y., Nomura, T., Hashimoto, N., and Hashimoto, T.: Bipolar charging and neutralization of nanometer-sized aerosol particles, J. Aerosol Sci., 28, 1479–1490, 1997.

Berresheim, H., Elste, T., Plass-Dulmer, C., Eiseleb, F. L., and Tannerb, D. J.: Chemical ionization mass spectrometer for long-term measurements of atmospheric OH and H_2SO_4, Int. J. Mass spectrom., 202, 91–109, 2000.

Birmili, W., Berresheim, H., Plass-Dülmer, C., Elste, T., Gilge, S., Wiedensohler, A., and Uhrner, U.: The Hohenpeissenberg aerosol formation experiment (HAFEX): a long-term study including size-resolved aerosol, H_2SO_4, OH, and monoterpenes measurements, Atmos. Chem. Phys., 3, 361–376, doi:10.5194/acp-3-361-2003, 2003.

Cantrell, C. A.: Technical Note: Review of methods for linear least-squares fitting of data and application to atmospheric chemistry problems, Atmos. Chem. Phys., 8, 5477–5487, doi:10.5194/acp-8-5477-2008, 2008.

Charlson, R. J., Schwartz, S. E., Hales, J. M., Cess, R. D., Coakley, J. A., Hansen, J. E., and Hofmann, D. J.: Climate forcing by anthropogenic aerosols, Science, 255, 423–430, 1992.

Fiedler, V., Dal Maso, M., Boy, M., Aufmhoff, H., Hoffmann, J., Schuck, T., Birmili, W., Hanke, M., Uecker, J., Arnold, F., and Kulmala, M.: The contribution of sulphuric acid to atmospheric particle formation and growth: a comparison between boundary layers in Northern and Central Europe, Atmos. Chem. Phys., 5, 1773–1785, doi:10.5194/acp-5-1773-2005, 2005.

Friedlander, S. K.: Smoke, Dust, and Haze, Wiley, New York, 1977.

Fuchs, N. A.: The Mechanics of Aerosols, Pergamon Press, New York, 1964.

Gelbard, F. and Seinfeld, J. H.: Numerical solution of the dynamic equation for particulate systems, J. Comp. Phys., 28, 357–375, 1978.

Heisler, S. L. and Friedlander, S. K.: Gas-to-particle conversion in photochemical smog: Aerosol growth laws and mechanisms for organics, Atmos. Environ., 11, 157–168, 1977.

Hirsikko, A., Laakso, L., Horrak, U., Aalto, P. P., Kerminen, V., and Kulmala, M.: Annual and size dependent variation of growth rates and ion concentrations in boreal forest, Boreal Environ. Res., 10, 357–369, 2005.

Iida, K., Stolzenburg, M. R., McMurry, P. H., and Smith, J. N.: Estimating nanoparticle growth rates from size-dependent charged fractions: analysis of new particle formation events in Mexico City, J. Geophys. Res., 113, D05207, doi:10.1029/2007JD009260, 2008.

Iida, K., Stolzenburg, M. R., and McMurry, P. H.: Effect of working fluid on sub-2 nm particle detection with a laminar flow ultrafine condensation particle counter, Aerosol Sci. Technol., 43, 81–96, 2009.

Jefferson, A., Eisele, F. L., Ziemann, P. J., Weber, R. J., Marti, J. J., and McMurry, P. H.: Measurements of the H_2SO_4 mass accommodation coefficient onto polydisperse aerosol, J. Geophys. Res., 102, 19021–19019, 1997.

Jiang, J., Chen, M., Kuang, C., Attoui, M., and McMurry, P. H.: Electrical Mobility Spectrometer Using a Diethylene Glycol Condensation Particle Counter for Measurement of Aerosol Size Distributions Down to 1 nm, Aerosol Sci. Technol., 45, 510–521, doi:10.1080/02786826.2010.547538, 2011a.

Jiang, J., Zhao, J., Chen, M., Eisele, F. L., Scheckman, J., Williams, B. J., Kuang, C., and McMurry, P. H.: First Measurements of Neutral Atmospheric Cluster and 1-2 nm Particle Number Size Distributions During Nucleation Events, Aerosol Sci. Technol., 45, 2–5, doi:10.1080/02786826.2010.546817, 2011b.

Kerminen, V. M. and Kulmala, M.: Analytical formulae connecting the "real" and the "apparent" nucleation rate and the nuclei number concentration for atmospheric nucleation events, J. Aerosol Sci., 33, 609–622, 2002.

Kerminen, V. M., Lihavainen, H., Komppula, M., Viisanen, Y., and Kulmala, M.: Direct observational evidence linking atmospheric aerosol formation and cloud droplet activation, Geophys. Res. Lett., 32, L14803, doi:10.1029/2005GL023130, 2005.

Knutson, E. O.: Extended electric mobility method for measuring aerosol particle size and concentration, in: Fine Particles: Aerosol Generation, Measurement, Sampling, and Analysis, edited by: Liu, B. Y. H., Academic Press, New York, 739–762, 1976.

Kuang, C., McMurry, P. H., and McCormick, A. V.: Determination of cloud condensation nuclei production from measured new particle formation events, Geophys. Res. Lett., 36, L09822, doi:10.1029/2009GL037584, 2009.

Kuang, C., Riipinen, I., Sihto, S.-L., Kulmala, M., McCormick, A. V., and McMurry, P. H.: An improved criterion for new particle formation in diverse atmospheric environments, Atmos. Chem. Phys., 10, 8469–8480, doi:10.5194/acp-10-8469-2010, 2010.

Kuang, C., Chen, M., McMurry, P. H., and Wang, J.: Modification of Laminar Flow Ultrafine Condensation Particle Counters for the Enhanced Detection of 1 nm Condensation Nuclei, Aerosol Sci. Technol., 46, 309–315, doi:10.1080/02786826.2011.626815, 2012.

Kulmala, M., Kerminen, V. M., Anttila, T., Laaksonen, A., and O'Dowd, C. D.: Organic aerosol formation via sulphate cluster activation, J. Geophys. Res., 109, D04205, doi:10.1029/2003JD003961, 2004a.

Kulmala, M., Laakso, L., Lehtinen, K. E. J., Riipinen, I., Dal Maso, M., Anttila, T., Kerminen, V.-M., Hõrrak, U., Vana, M., and Tammet, H.: Initial steps of aerosol growth, Atmos. Chem. Phys., 4, 2553–2560, doi:10.5194/acp-4-2553-2004, 2004b.

Kulmala, M., Vehkamäki, H., Petäjä, T., Dal Maso, M., Lauri, A., Kerminen, V. M., Birmili, W., and McMurry, P. H.: Formation and growth rates of ultrafine atmospheric particles: a review of observations, J. Aerosol Sci., 35, 143–176, 2004c.

Larriba, C., Hogan, C. J., Attoui, M., Borrajo, R., Garcia, J. F., and de la Mora, J. F.: The Mobility–Volume Relationship below 3.0 nm Examined by Tandem Mobility-Mass Measurement, Aerosol Sci. Technol., 45, 453–467, 2011.

Lehtinen, K. E. J. and Kulmala, M.: A model for particle formation and growth in the atmosphere with molecular resolution in size, Atmos. Chem. Phys., 3, 251–257, doi:10.5194/acp-3-251-2003, 2003.

Lehtinen, K. E. J., Rannik, Ü., Petäjä, T., Kulmala, M., and Hari, P.: Nucleation rate and vapor concentration estimations using a least squares aerosol dynamics method, J. Geophys. Res., 109, D21209, doi:10.1029/2004JD004893, 2004.

Lehtinen, K. E. J., Dal Maso, M., Kulmala, M., and Kerminen, V. M.: Estimating nucleation rates from apparent particle formation rates and vice versa: Revised formulation of the Kerminen-Kulmala equation, J. Aerosol Sci., 38, 988–994, 2007.

Lehtipalo, K., Sipilä, M., Junninen, H., Ehn, M., Berndt, T., Kajos, M. K., Worsnop, D. R., Petäjä, T., and Kulmala, M.: Observations of Nano-CN in the Nocturnal Boreal Forest, Aerosol Sci. Technol., 45, 499–509, 2011.

Lihavainen, H., Kerminen, V. M., Komppula, M., Hatakka, J., Aaltonen, V., Kulmala, M., and Viisanen, Y.: Production of "potential" cloud condensation nuclei associated with atmospheric new-particle formation in northern Finland, J. Geophys. Res., 108, 4782, doi:10.1029/2003jd003887, 2003.

Mäkelä, J. M., Dal Maso, M., Pirjola, L., Keronen, P., Laakso, L., Kulmala, M., and Laaksonen, A.: Characteristics of the atmospheric particle formation events observed at a boreal forest site in southern Finland, Boreal Environ. Res., 5, 299–313, 2000.

Mäkelä, J. M., Yli-Koivisto, S., Hiltunen, V., Seidl, W., Swietlicki, E., Teinilä, K., Sillanpää, M., Koponen, I. K., Paatero, J., Rosman, K., and Hämeri, K.: Chemical composition of aerosol during particle formation events in boreal forest, Tellus B, 53, 380–393, 2001.

Manninen, H. E., Nieminen, T., Riipinen, I., Yli-Juuti, T., Gagné, S., Asmi, E., Aalto, P. P., Petäjä, T., Kerminen, V.-M., and Kulmala, M.: Charged and total particle formation and growth rates during EUCAARI 2007 campaign in Hyytiälá, Atmos. Chem.

Phys., 9, 4077–4089, doi:10.5194/acp-9-4077-2009, 2009.

McMurry, P. H.: New particle formation in the presence of an aerosol: rates, time scales, and sub-0.01 µm size distributions, J. Colloid Interface Sci., 95, 72–80, 1983.

McMurry, P. H.: A review of atmospheric aerosol measurements, Atmos. Environ., 34, 1959–1999, 2000.

McMurry, P. H. and Friedlander, S. K.: Aerosol formation in reacting gases: Relation of surface area to rate of gas-to-particle conversion, J. Colloid Interface Sci., 64, 248–257, 1977.

McMurry, P. H. and Grosjean, D.: Photochemical formation of organic aerosols: growth laws and mechanisms, Atmos. Environ., 19, 1445–1451, 1985.

McMurry, P. H. and Wilson, J. C.: Growth laws for the formation of secondary ambient aerosols: implications for chemical conversion mechanisms, Atmos. Environ., 16, 121–134, 1982.

McMurry, P. H., Fink, M., Sakurai, H., Stolzenburg, M. R., Mauldin, R. L., Smith, J., Eisele, F., Moore, K., Sjostedt, S., Tanner, D., Huey, L. G., Nowak, J. B., Edgerton, E., and Voisin, D.: A criterion for new particle formation in the sulfur-rich Atlanta atmosphere, J. Geophys. Res., 110, D22S02, doi:10.1029/2005JD005901, 2005.

Metzger, A., Verheggen, B., Dommen, J., Duplissy, J., Prevot, A. S. H., Weingartner, E., Riipinen, I., Kulmala, M., Spracklen, D. V., and Carslaw, K. S.: Evidence for the role of organics in aerosol particle formation under atmospheric conditions, P. Natl. Acad. Sci. USA, 107, 6646, doi:10.1073/pnas.0911330107, 2010.

Neri, F., Saitta, G., and Chiofalo, S.: An accurate and straightforward approach to line regression analysis of error-affected experimental data, Journal of Physics E: Scientific Instruments, 22, 215–217, 1989.

Nieminen, T., Lehtinen, K. E. J., and Kulmala, M.: Sub-10 nm particle growth by vapor condensation – effects of vapor molecule size and particle thermal speed, Atmos. Chem. Phys., 10, 9773–9779, doi:10.5194/acp-10-9773-2010, 2010.

O'Dowd, C. D., Aalto, P., Hameri, K., Kulmala, M., and Hoffmann, T.: Atmospheric particles from organic vapours, Nature, 416, 497–498, 2002.

Pierce, J. R. and Adams, P. J.: Efficiency of cloud condensation nuclei formation from ultrafine particles, Atmos. Chem. Phys., 7, 1367–1379, doi:10.5194/acp-7-1367-2007, 2007.

Pierce, J. R. and Adams, P. J.: Uncertainty in global CCN concentrations from uncertain aerosol nucleation and primary emission rates, Atmos. Chem. Phys., 9, 1339–1356, doi:10.5194/acp-9-1339-2009, 2009.

Premnath, V., Oberreit, D., and Hogan Jr, C. J.: Collision-Based Ionization: Bridging the Gap between Chemical Ionization and Aerosol Particle Diffusion Charging, Aerosol Sci. Technol., 45, 712–726, doi:10.1080/02786826.2011.556683, 2011.

Reischl, G. P., Makela, J. M., Karch, R., and Necid, J.: Bipolar charging of ultrafine particles in the size range below 10 nm, J. Aerosol Sci., 27, 931–949, 1996.

Riipinen, I., Sihto, S.-L., Kulmala, M., Arnold, F., Dal Maso, M., Birmili, W., Saarnio, K., Teinilä, K., Kerminen, V.-M., Laaksonen, A., and Lehtinen, K. E. J.: Connections between atmospheric sulphuric acid and new particle formation during QUEST III–IV campaigns in Heidelberg and Hyytiälä, Atmos. Chem. Phys., 7, 1899–1914, doi:10.5194/acp-7-1899-2007, 2007.

Seinfeld, J. H. and Pandis, S. N.: Atmospheric Chemistry and Physics: From Air Pollution to Climate Change, Second ed.,

John Wiley & Sons, New York, 2006.

Sihto, S.-L., Kulmala, M., Kerminen, V.-M., Dal Maso, M., Petäjä, T., Riipinen, I., Korhonen, H., Arnold, F., Janson, R., Boy, M., Laaksonen, A., and Lehtinen, K. E. J.: Atmospheric sulphuric acid and aerosol formation: implications from atmospheric measurements for nucleation and early growth mechanisms, Atmos. Chem. Phys., 6, 4079–4091, doi:10.5194/acp-6-4079-2006, 2006.

Sipilä, M., Lehtipalo, K., Attoui, M., Neitola, K., Petäjä, T., Aalto, P. P., O'Dowd, C. D., and Kulmala, M.: Laboratory Verification of PH-CPC's Ability to Monitor Atmospheric Sub-3 nm Clusters, Aerosol Sci. Technol., 43, 126–135, 2009.

Smith, J. N. and Rathbone, G. J.: Carboxylic acid characterization in nanoparticles by thermal desorption chemical ionization mass spectrometry, Int. J. Mass spectrom., 274, 8–13, 2008.

Smith, J. N., Moore, K. F., McMurry, P. H., and Eisele, F. L.: Atmospheric measurements of sub-20 nm diameter particle chemical composition by thermal desorption chemical ionization mass spectrometry, Aerosol Sci. Technol., 38, 100–110, 2004.

Smith, J. N., Moore, K. F., Eisele, F. L., Voisin, D., Ghimire, A. K., Sakurai, H., and McMurry, P. H.: Chemical composition of atmospheric nanoparticles during nucleation events in Atlanta, J. Geophys. Res.-Atmos., 110, D22S03, doi:10.1029/2005JD005912, 2005.

Smith, J. N., Dunn, M. J., VanReken, T. M., Iida, K., Stolzenburg, M. R., McMurry, P. H., and Huey, L. G.: Chemical composition of atmospheric nanoparticles formed from nucleation in Tecamac, Mexico: evidence for an important role for organic species in nanoparticle growth, Geophys. Res. Lett., 35, L04808, doi:10.1029/2007GL032523, 2008.

Smith, J. N., Barsanti, K. C., Friedli, H. R., Ehn, M., Kulmala, M., Collins, D. R., Scheckman, J. H., Williams, B. J., and McMurry, P. H.: Observations of aminium salts in atmospheric nanoparticles and possible climatic implications, P. Natl. Acad. Sci. USA, 15, 6634–6639, 2010.

Spracklen, D. V., Carslaw, K. S., Kulmala, M., Kerminen, V. M., Sihto, S.-L., Riipinen, I., Merikanto, J., Mann, G. W., Chipperfield, M. P., Wiedensohler, A., Birmili, W., and Lihavainen, H.: Contribution of particle formation to global cloud condensation nuclei concentrations, Geophys. Res. Lett., 35, L06808, doi:10.1029/2007GL033038, 2008.

Spracklen, D. V., Carslaw, K. S., Merikanto, J., Mann, G. W., Reddington, C. L., Pickering, S., Ogren, J. A., Andrews, E., Baltensperger, U., Weingartner, E., Boy, M., Kulmala, M., Laakso, L., Lihavainen, H., Kivekäs, N., Komppula, M., Mihalopoulos, N., Kouvarakis, G., Jennings, S. G., O'Dowd, C., Birmili, W., Wiedensohler, A., Weller, R., Gras, J., Laj, P., Sellegri, K., Bonn, B., Krejci, R., Laaksonen, A., Hamed, A., Minikin, A., Harrison, R. M., Talbot, R., and Sun, J.: Explaining global surface aerosol number concentrations in terms of primary emissions and particle formation, Atmos. Chem. Phys., 10, 4775–4793, doi:10.5194/acp-10-4775-2010, 2010.

Stolzenburg, M. R. and McMurry, P. H.: An Ultrafine Aerosol Condensation Nucleus Counter, Aerosol Sci. Technol., 14, 48–65, 1991.

Stolzenburg, M. and McMurry, P.: Equations Governing Single and Tandem DMA Configurations and a New Lognormal Approximation to the Transfer Function, Aerosol Sci. Technol., 42, 421–432, 2008.

Stolzenburg, M. R., McMurry, P. H., Sakurai, H., Smith, J. N., Mauldin, R. L., Eisele, F. L., and Clement, C. F.: Growth rates of freshly nucleated atmospheric particles in Atlanta, J. Geophys. Res., 110, D22S05, doi:10.1029/2005JD005935, 2005.

Verheggen, B. and Mozurkewich, M.: An inverse modeling procedure to determine particle growth and nucleation rates from measured aerosol size distributions, Atmos. Chem. Phys., 6, 2927–2942, doi:10.5194/acp-6-2927-2006, 2006.

Viggiano, A. A., Seeley, J. V., Mundis, P. L., Williamson, J. S., and Morris, R. A.: Rate Constants for the Reactions of $XO^{3-}(H_2O)_n$ (X= C, HC, and N) and $NO^{3-}(HNO_3)_n$ with H_2SO_4: Implications for Atmospheric Detection of H_2SO_4, J. Phys. Chem. A, 101, 8275–8278, 1997.

Wang, M. and Penner, J. E.: Aerosol indirect forcing in a global model with particle nucleation, Atmos. Chem. Phys., 9, 239–260, doi:10.5194/acp-9-239-2009, 2009.

Weber, R. J., Marti, J. J., McMurry, P. H., Eisele, F. L., Tanner, D. J., and Jefferson, A.: Measured atmospheric new particle formation rates: Implications for nucleation mechanisms, Chem. Eng. Commun., 151, 53–64, 1996.

Weber, R. J., Marti, J. J., McMurry, P. H., Eisele, F. L., Tanner, D. J., and Jefferson, A.: Measurements of new particle formation and ultrafine particle growth rates at a clean continental site, J. Geophys. Res., 102, 4375–4385, 1997.

Wiedensohler, A.: An Approximation of the Bipolar Charge-Distribution for Particles in the Sub-Micron Size Range, J. Aerosol Sci., 19, 387–389, 1988.

Williamson, J. H.: Least-squares fitting of a straight line, CaJPh, 46, 1845–1847, 1968.

Woo, K. S., Chen, D. R., Pui, D. Y. H., and McMurry, P. H.: Measurement of Atlanta aerosol size distributions: observations of ultrafine particle events, Aerosol Sci. Technol., 34, 75–87, 2001.

Yli-Juuti, T., Nieminen, T., Hirsikko, A., Aalto, P. P., Asmi, E., Hõrrak, U., Manninen, H. E., Patokoski, J., Dal Maso, M., Petäjä, T., Rinne, J., Kulmala, M., and Riipinen, I.: Growth rates of nucleation mode particles in Hyytiälä during 2003–2009: variation with particle size, season, data analysis method and ambient conditions, Atmos. Chem. Phys., 11, 12865–12886, doi:10.5194/acp-11-12865-2011, 2011.

Zhao, J., Eisele, F. L., Titcombe, M., Kuang, C., and McMurry, P. H.: Chemical ionization mass spectrometric measurements of atmospheric neutral clusters using the cluster-CIMS, J. Geophys. Res., 115, D08205, doi:10.1029/2009JD012606, 2010.